Conference Applications of Mathematics 2012
in honor of the 60th birthday of Michal Křížek.
Institute of Mathematics AS CR, Prague 2012

ON USING ARTIFICIAL COMPRESSIBILITY METHOD FOR SOLVING TURBULENT FLOWS

Petr Louda[1], Karel Kozel[1], Jaromír Příhoda[2]

[1] Czech Technical University in Prague, Fac. of Mech. Engineering
Karlovo nám. 13, Praha 2, Czech Republic
petr.louda@fs.cvut.cz, karel.kozel@fs.cvut.cz
[2] Institute of Thermomechanics
Doleškova 5, Praha 8, Czech Republic
prihoda@it.cas.cz

Abstract

In this work, artificial compressibility method is used to solve steady and unsteady flows of viscous incompressible fluid. The method is based on implicit higher order upwind discretization of Navier-Stokes equations. The extension for unsteady simulation is considered by increasing artificial compressibility parameter or by using dual time stepping. The methods are tested on laminar flow around circular cylinder and used to simulate turbulent unsteady flows by URANS approach. The simulated cases are synthetic jet and flow in a branched channel.

1. Introduction

The work deals with numerical solution of incompressible viscous (laminar and turbulent) unsteady flows. The solved cases include flows with self-induced unsteadiness – laminar flow around circular cylinder, turbulent flow through branched channel, and unsteadiness caused by periodic forcing – synthetic free jet.

The algorithm used in this work is based on artificial compressibility method. The idea, proposed by Chorin [2], is to complete continuity equation by a pressure time derivative $\frac{1}{\beta^2}\frac{\partial p}{\partial t}$ and then use some numerical scheme for compressible flow computation. With steady boundary conditions and time dependent method steady solution may be achieved for $t \to \infty$. An extension for unsteady simulation is achieved by introducing dual time and using implicit discretization for both physical and artificial time.

2. Mathematical model

The governing equations are Navier-Stokes (NS) equations for incompressible fluid (density $\rho = const$) in Cartesian coordinates

$$\begin{aligned} \frac{\partial u_i}{\partial x_i} &= 0 \\ \frac{\partial u_i}{\partial t} + \frac{\partial u_i u_j}{\partial x_j} &= -\frac{1}{\rho}\frac{\partial p}{\partial x_i} + \nu \frac{\partial}{\partial x_j}\left(\frac{\partial u_i}{\partial x_j} + \frac{\partial u_j}{\partial x_i}\right) \end{aligned} \tag{1}$$

where u_i is velocity vector, p static pressure and ν kinematic viscosity of the fluid. A convenient time marching algorithm for NS equations for incompressible flow can be achieved by artificial compressibility method. In its simplest form, only the continuity equation is modified by pressure time derivative

$$\frac{1}{\beta^2}\frac{\partial (p/\rho)}{\partial t} + \frac{\partial u_i}{\partial x_i} = 0, \tag{2}$$

where β is positive parameter. The inviscid part of modified NS equations is now fully hyperbolic and can be solved by standard methods for hyperbolic conservation laws. The system including continuity equation and two momentum equations in 3D can be written as

$$\begin{aligned} &\Gamma \frac{\partial W}{\partial t} + Rez(W) = 0, \quad \Gamma = diag[\beta^{-2}, 1, 1, 1],\ W = col[p/\rho, u_1, u_2, u_3], \\ &(x_1, x_2, x_3) \in D,\ t \in (0, \infty),\ Rez(W) = \frac{\partial (u_i u_j)}{\partial x_j} + \frac{\partial (p/\rho)}{\partial x_i} - \nu \frac{\partial}{\partial x_j}\left(\frac{\partial u_i}{\partial x_j} + \frac{\partial u_j}{\partial x_i}\right) \end{aligned} \tag{3}$$

where W is vector of unknown pressure and velocity components, and steady residual $Rez(W)$ is zero for steady solution. However, the divergence free velocity field is not achieved before steady state at which $\partial p/\partial t = 0$. In unsteady case, the velocity divergence error may have negligible impact on relevant flow parameters if the β^2 is large enough.

Other possibility of dealing with unsteadiness is to introduce artificial (dual, iterative) time τ and apply the artificial compressibility method in this time:

$$\begin{aligned} &\Gamma \frac{\partial W}{\partial \tau} + Rez^{uns}(W) = 0, \quad Rez^{uns}(W) = R\frac{\partial W}{\partial t} + Rez(W), \\ &R = diag[0, 1, 1, 1],\ (x_1, x_2, x_3) \in D, \quad t \in (t_n, t_{n+1}), \quad \tau \in (0, \infty) \end{aligned} \tag{4}$$

where $Rez^{uns}(W)$ is unsteady residual. The steady state in τ now should be achieved at each physical time level t.

2.1. Turbulence modelling

In order to simulate turbulent flows the Reynolds averaging procedure is used leading to the Reynolds-averaged Navier-Stokes (RANS) system of equations. For unsteady simulation it formally becomes URANS (unsteady RANS) approach. The

physical meaning is maintained if the simulated unsteadiness is far enough from turbulent unsteadiness with time and length scale respectively

$$\tau_t \approx \frac{k}{\epsilon}, \quad l_t \approx \frac{k^{3/2}}{\epsilon}, \tag{5}$$

where k is turbulent energy and ϵ turbulent dissipation rate. For unsteady flow with periodic forcing the averaging is phase averaging. The averaged equations formally differ from Navier-Stokes equations by additional momentum transport expressed by the Reynolds stress tensor. In this work, the Reynolds stress is modelled using Shear Stress Transport (SST) model [5] and an explicit algebraic Reynolds stress model (EARSM) [9, 3]. In the SST model, the extended eddy-viscosity assumption is used to express the Reynolds stress, while in EARSM a constitutive relation contains terms up to fourth order in terms of velocity gradient. Both turbulence models require solving a system of k-ω equations for turbulent scales ($\omega \sim \epsilon/k$).

2.2. Numerical methods

The stability limitation for an explicit artificial compressibility method requires $\Delta t \sim L/\beta$, where L is minimum step size of a numerical grid. In view of the necessity to increase β and of application to simulation of viscous flows, an implicit three-layer scheme of second order accuracy is used. For single time method, the scheme reads

$$\Gamma \frac{3W_{i,j,k}^{n+1} - 4W_{i,j,k}^{n} + W_{i,j,k}^{n-1}}{2\Delta t} + Rez(W)_{i,j,k}^{n+1} = 0. \tag{6}$$

For dual time method, the scheme is backward Euler in artificial time (superscript μ)

$$\Gamma \frac{W_{i,j,k}^{\mu+1} - W_{i,j,k}^{\mu}}{\Delta \tau} + R \frac{3W_{i,j,k}^{\mu+1} - 4W_{i,j,k}^{n} + W_{i,j,k}^{n-1}}{2\Delta t} + Rez(W)_{i,j,k}^{\mu+1} = 0. \tag{7}$$

The steady residuals are computed by a cell-centered finite volume method with quadrilateral or hexahedral finite volumes in 2D and 3D, respectively. The discretization of convective terms uses third order accurate van Leer upwind interpolation. Pressure gradient is computed by central approximation. The viscous terms are approximated using 2nd order central scheme, with cell face derivatives computed on a dual grid of quadrilaterals/ octahedrons in 2D/ 3D constructed over each face of primary grid using vertices of the face and centres of two adjacent finite volumes.

3. Numerical results

3.1. Laminar flow around a cylinder

In this section, 2D laminar flow around the circular cylinder is considered. The first test case is circular cylinder of diameter D placed excentrically inside channel [6]. The Reynolds number $Re = UD/\nu = 100$, where U is bulk inlet velocity. At this Reynolds number, unsteady periodic flow evolves due to the vortex shedding on

	reference [6]	$\beta = U$	$\beta = 10U$	dual time ($\beta = U$)
$\max(c_D)$	3.10–3.28	3.39	3.27	3.10
$\max(c_L)$	0.99–1.01	0.77	1.09	0.98
$St = Df/U$	0.295–0.305	0.196	0.288	0.294

Table 1: Drag, lift and the Strouhal number for flow around cylinder in channel.

Re	47	50	60	80	100	120	140
St	0.1336	0.1362	0.1438	0.1547	0.1642	0.1733	0.1821
C_D (mean)	1.55	1.53	1.50	1.43	1.36	1.34	1.34
C_L (ampl.)	0.15	0.18	0.22	0.22	0.23	0.34	0.45

Table 2: Strouhal number, drag and lift coefficients for cylinder in free space.

the cylinder. The computed force on the cylinder (F_D, F_L) is expressed by drag coefficient $C_D = 2F_D/(\rho U^2 D)$ and lift coefficient $C_L = 2F_L/(\rho U^2 D)$ are compared with reference compilation [6] as well as the Strouhal number $St = D/(TU)$, where T is period of the force, see Tab. 1. For single time method with $\beta = U$, the Strouhal number is too small. In the case of $\beta = 10U$, the results improve. However this value of β was about the maximum for an acceptable time step ($\Delta t = 0.02D/U$). The results of dual time stepping method using $\beta = U, \Delta t = 0.06D/U$ are clearly best, however at the cost of higher CPU time. The time evolution of drag and lift for the mentioned cases are shown in Figs.1, 2 and 3.

The evolution of L_2-norm of steady and unsteady residual is shown in Fig. 4 ($Re = 100$). The convergence of pressure is worst, which is typical for this form of artificial compressibility method. The behaviour does not change for $\beta = \sqrt{0.1}$ or $\sqrt{10}$ either.

Next we consider cylinder in a free stream of velocity U. The cylinder is placed in the middle of the computational domain of size $40D$(streamwise) $\times$ $100D$. The results are achieved with dual time method with $\beta = U, \Delta t = 0.06D/U$.

Figure 5 shows dependency of the Strouhal number (frequency) of vortex shedding for different Reynolds numbers, in comparison with empirical corelation $St = 0.266 - 1.016/\sqrt{Re}$ [10]. The critical Reynolds number where vortex shedding starts is recently measured at $Re = 47.5 \pm 0.7$ [10]. In our computation, the flow is steady for $Re = 30$, unsteady but non-periodic for $Re = 40$ and periodic at $Re = 47$ (shown in Fig. 5). However for lower Re the computed shedding frequency is higher than the empirical correlation. Another computational attempt [8], probably on finer grid, shows good agreement with experiment however predicted much higher critical Re. The results are summarized in Tab. 2. An example of flow-field ($Re = 100$) is shown in Fig. 6.

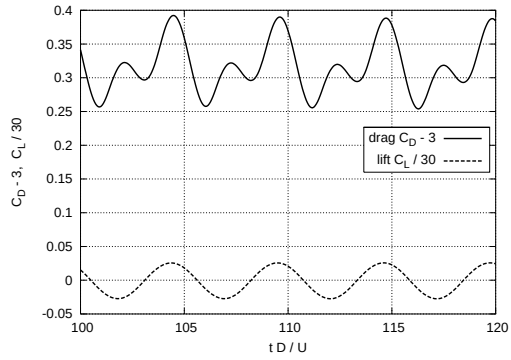

Figure 1: Laminar flow around cylinder, $\beta = U$.

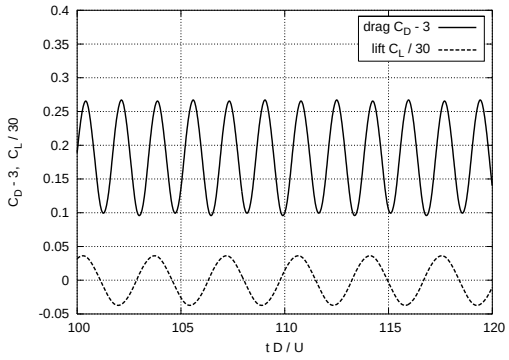

Figure 2: Laminar flow around cylinder, $\beta = 10U$.

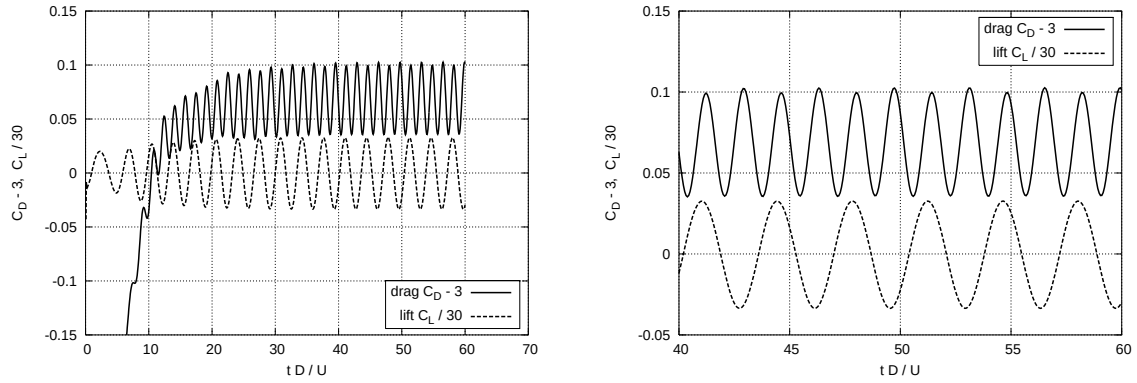

Figure 3: Laminar flow around cylinder, dual time stepping. Left: evolution from initial state, right: zoom of periodic flow.

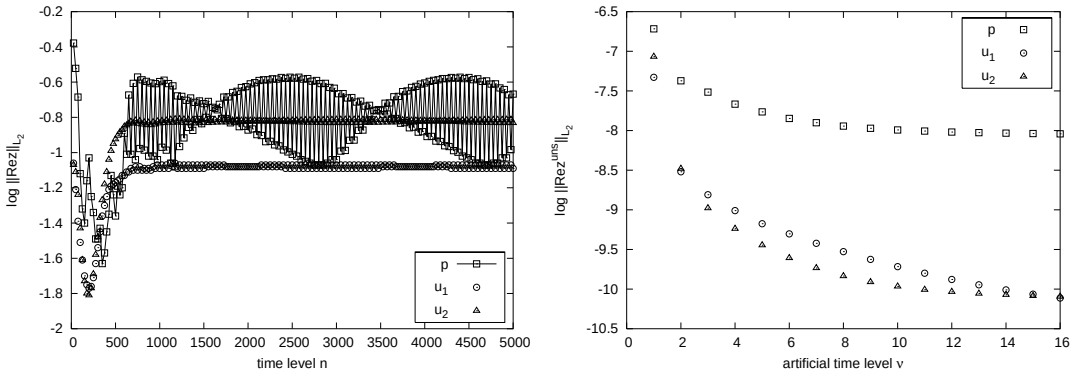

Figure 4: Laminar flow around cylinder, convergence history for dual time method. Left: steady residual showing that we have unsteady solution, right: typical history of unsteady residual showing convergence for unsteady flow between time t_n and t_{n+1}.

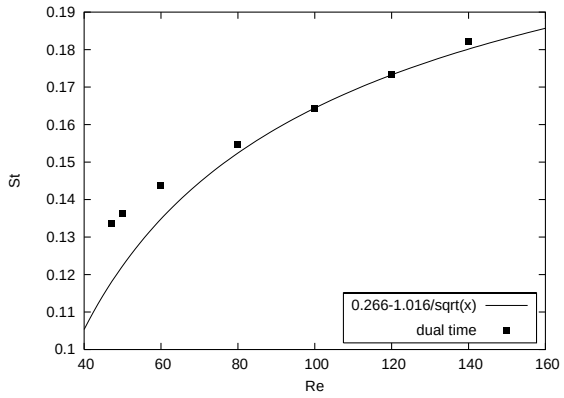

Figure 5: Reynolds number dependence of the Strouhal number.

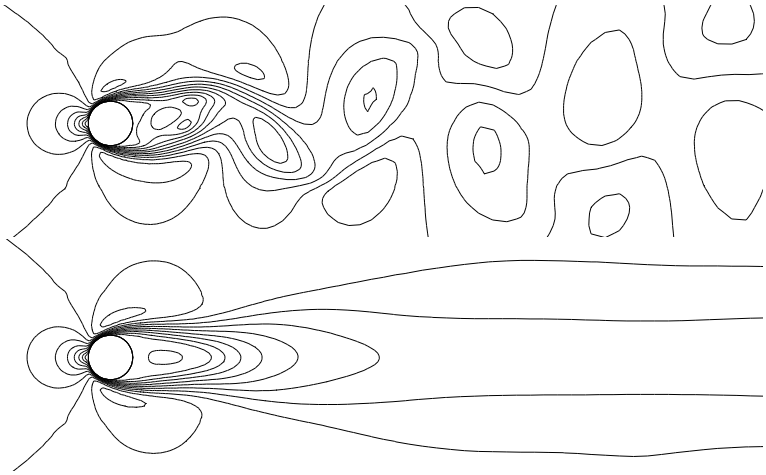

Figure 6: Isolines of velocity around cylinder in free space. Above: instantaneous velocity, below: time averaged velocity.

3.2. Turbulent 3D synthetic free jet flow

In this part, we consider the synthetic jet generated by periodical inflow/outflow with zero mean value in the circular nozzle [7]. The Reynolds number from nozzle diameter and velocity amplitude $Re = U_{max}D/\nu = 13\,325$. Turbulence is modelled by the SST model. We used dual time stepping method with $\beta = U_{max}$ and $\Delta t = T/72$ with forcing period $T = 1/(75\text{Hz})$. The computed instantaneous velocity on jet axis is compared with measured [7] phase averaged velocity in Fig. 9. For larger x/D, the flowfield corresponds to steady free jet. Next Fig. 10 shows time averaged velocity on jet axis. The computational results achieved using Fluent code with axisymmetrical formulation in [7] are also shown. The velocity on the axis by Fluent decreases too fast, which suggests higher spreading rate than in experiment. The time averaged velocity profiles exhibit self-similarity already in the unsteady region. The computational results, Fig. 11, have this feature except for small distance to the

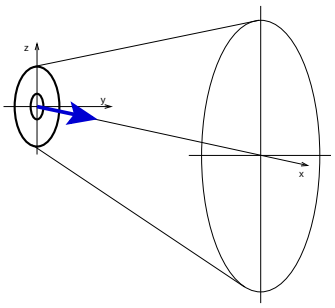

Figure 7: Solution domain for synthetic jet.

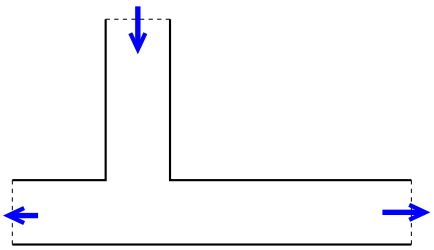

Figure 8: Solution domain for channel junction.

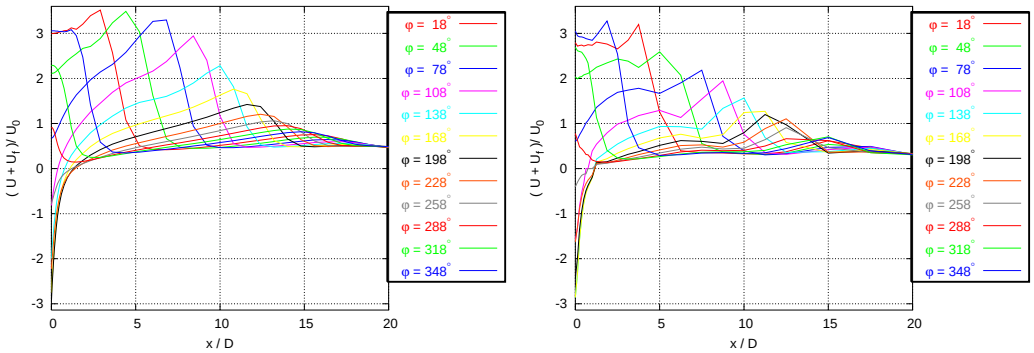

Figure 9: Phase averaged velocity on jet axis. Left: computation, right: measurement.

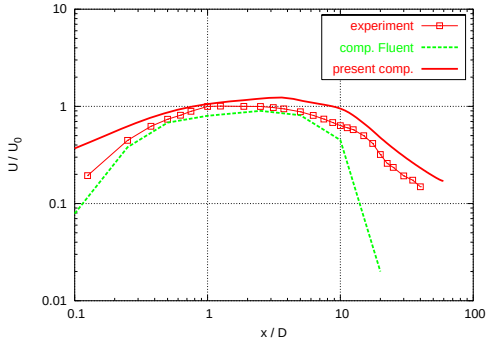

Figure 10: Time averaged velocity on the jet axis.

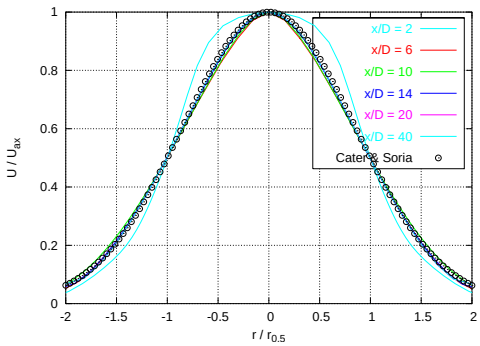

Figure 11: Time averaged velocity profiles.

nozzle, where an approximate boundary condition again plays a role. In this figure, the $r_{0.5}$ denotes the radial distance from jet axis, where the velocity reaches half of the axial velocity. Velocity profiles moreover agree well with empirical correlation $U/U_{ax} = \exp[-\ln(2)(r/r_{0.5})^2]$ according to [1].

3.3. Turbulent 3D flow in channel with branch

Here, turbulent flow in a channel with perpendicular branch is considered. In ref. [4], the channel had 1 inlet in the main channel and 2 outlets: from main channel and from the branch. In the following the case with inlet through branch and 2 outlets from the main channel is presented. The solution domain as well as finite volume grid is same as in [4]. The Reynolds number computed from inlet diameter and bulk velocity is $Re = 140\,000$. Different distribution of outflow into the outlets can be prescribed. The target flow rates are achieved using 2 conditions for pressure in the outlets:

α) "do-nothing"-like condition

$$\mu \frac{\partial u}{\partial n} - p = p_{ref} \tag{8}$$

where u is velocity component normal to the outlet plane, μ dynamic viscosity, p pressure and p_{ref} an arbitrary constant

β) correction for target flow rate U_{bt}

$$\frac{\partial p}{\partial n} = -\frac{U_{bt} - U_b}{\Delta t} \tag{9}$$

where U_b is flow rate at time t_n and $\Delta t = t_{n+1} - t_n$

The condition α can be used in 1 outlet only and needs to be combined with e.g. condition β. The condition β can be used in both outlets. Any of these 3 combinations worked comparably well in the simulated cases.

The distribution of outflow is 20:80, total flow-rate 5.5 l/s. In this configuration the simulation became unsteady and is interpreted in URANS sense. The Fig. 12 shows isolines of instantaneous and time averaged velocity near the junction. They seem quite similar. However, the next Fig. 13 shows that the resolved turbulent energy is comparable in magnitude to the turbulent energy from the turbulence model (color scale is same in both figures). The resolved unsteadiness is confined mainly to outlet channels. The comparison with PIV measurement is shown in Fig. 14 in terms of isolines of velocity.

4. Conclusions

In this work an artificial compressibility implicit upwind finite-volume method has been applied to unsteady flows of incompressible newtonian fluid. The computed

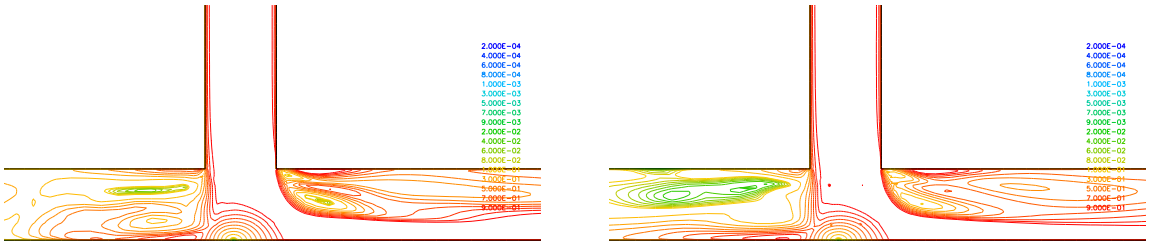

Figure 12: Isolines of instantaneous (left) and time averaged (right) velocity in the center-plane of T-channel.

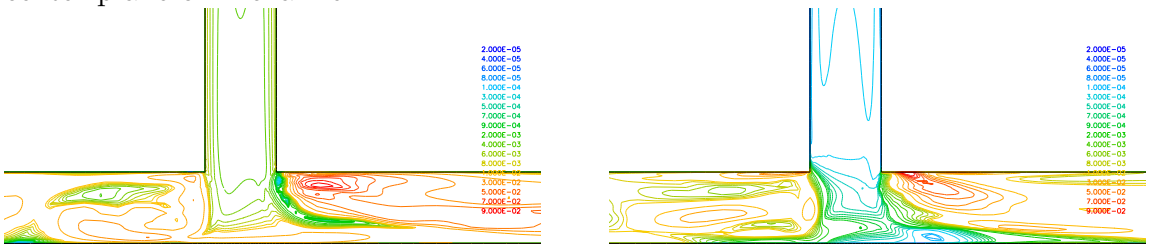

Figure 13: Isolines of modelled turbulent energy k (left) and resolved turbulent energy (right) in the center-plane of T-channel.

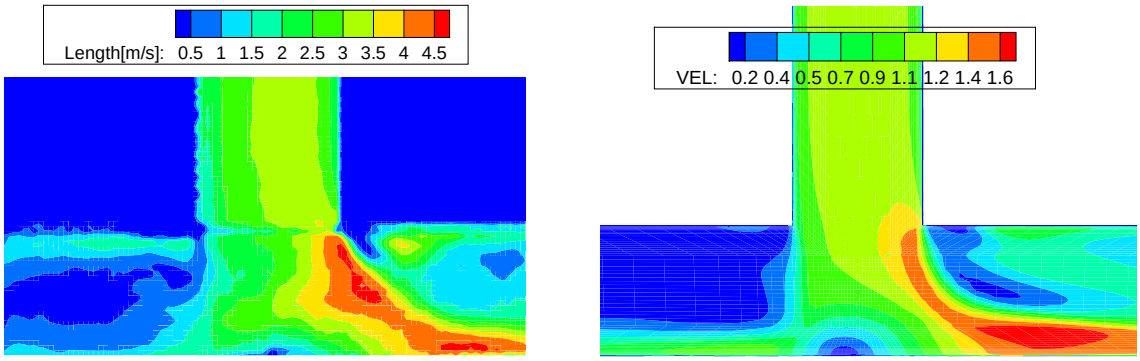

Figure 14: Velocity in the channel junction – experiment (left) and simulation (right).

cases included self-induced as well as forced unsteadiness. In single time method, the implicit discretization is necessary to overcome stability restriction when increasing artificial compressibility parameter. Although the computed lift force and the Strouhal number are satisfactory, the drag force is mis-predicted. The dual time stepping method is found more reliable and of sufficient accuracy also for studied 3D turbulent flows. The downside is that it is more CPU time consuming than single time method.

Acknowledgements

This work was supported by grants No. P101/10/1230, 101/09/1539 and P101/12/1271 of the Czech Science Foundation.

References

[1] Cater, J. E. and Soria, J.: The evolution of round zero-net-mass-flux jets. J. Fluid. Mech. **472** (2002), 167–200.

[2] Chorin, A. J.: A numerical method for solving incompressible viscous flow problems. J. of Computational Physics **2** (1967), 12–26.

[3] Hellsten, A.: New advanced k-ω turbulence model for high-lift aerodynamics. AIAA J. **43** (2005), 1857–1869.

[4] Louda, P., Kozel, K., Příhoda, J., Beneš, L., and Kopáček, T.: Numerical solution of incompressible flow through branched channels. Computers and Fluids **46** (2011), 318–324.

[5] Menter, F. R.: Two-equation eddy-viscosity turbulence models for engineering applications. AIAA J. **32** (1994), 1598–1605.

[6] Schäfer, M. and Turek, S.: Benchmark computations of laminar flow around a cylinder. In: *NNFM 52 "Flow simulation on high performance computers II"*, pp. 547–566. Vieweg, Braunschweig, 1996.

[7] Trávníček, Z., Vogel, J., Vít, T., and Maršík, F.: Flow field and mass transfer experimental and numerical studies of a synthetic impinging jet. In: *HEFAT2005, 4th International Conference on Heat Transfer, Fluid Mechanics, and Thermodynamics*. Cairo, Egypt, 2005 .

[8] Šponiar, D., Trávníček, Z., and Vogel, J.: Numerical simulation of the von Kármán vortex street. In: *Topical Problems of Fluid Mechanics 2007*. IT AS CR, 2007 .

[9] Wallin, S.: *Engineering turbulence modeling for CFD with a focus on explicit algebraic Reynolds stress models*. Ph.D. thesis, Royal Institute of Technology, Stockholm, 2000.

[10] Wang, A.B., Trávníček, Z., and Chia, K.C.: On the relationship of effective Reynolds number and Strouhal number for the laminar vortex shedding of a heated circular cylinder. Physics of Fluids **12** (2000), 1401–1410.